



Contents lists available at ScienceDirect

Spectrochimica Acta Part A: Molecular and Biomolecular Spectroscopy

journal homepage: www.journals.elsevier.com/spectrochimica-acta-part-a-molecular-and-biomolecular-spectroscopy



Dummy molecularly imprinted solid-phase extraction-SERS determination of AFB1 in peanut

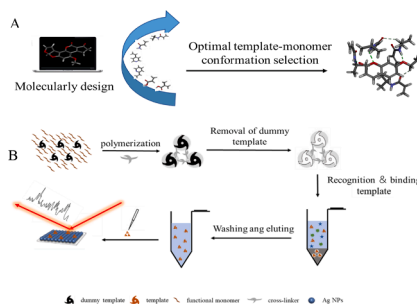
Li Fan, Qiong Zhang, Feng Wang*, Haifeng Yang*

The Education Ministry Key Lab of Resource Chemistry, Shanghai Key Laboratory of Rare Earth Functional Materials, Shanghai Municipal Education Committee Key Laboratory of Molecular Imaging Probes and Sensors, and Department of Chemistry, Shanghai Normal University, Shanghai 200234, PR China

HIGHLIGHTS

- DMISPE with good adsorption capacity and selectivity toward AFB1 were synthesized under the guidance of molecular simulation.
- A self-assembled thioctic-decorated AgNPs monolayer film was employed as a SERS-active substrate.
- The LOD of AFB1 detected by DMISPE-SERS was 0.1 $\mu\text{g/L}$.

GRAPHICAL ABSTRACT



ARTICLE INFO

Keywords:
AFB1
Discovery Studio
DMISPE
SERS

ABSTRACT

As a class I carcinogen, aflatoxin B1 (AFB1) contamination in foods and feeds accounts for 75 % of the total mycotoxin contamination. In this work, a simple and reliable surface-enhanced Raman spectroscopy (SERS) method for sensitive and selective detection of AFB1 in peanut samples integrated with dummy molecularly imprinted polymers (DMIPs) is developed. *N*-isopropylacrylamide (NIPAM) and 7-ethoxycoumarin (7-EOC) are chosen as monomer and dummy template, respectively and their ratio was screened through molecular design in both of kinetic and static adsorption views to form the optimal DMIPs. As-prepared dummy molecularly imprinted solid-phase extraction (DMISPE) could selectively enrich AFB1 from peanut samples. Finally, a liquid-liquid interface self-assembly constructed thioctic acid-decorated AgNPs monolayer film (TA-AgNPs MF) as a SERS-active substrate is employed to determine the amount of AFB1 eluted from DMISPE. SERS assay shows high detection sensitivity for AFB1 in peanut samples with limit of detection of 0.1 $\mu\text{g L}^{-1}$ and a linear concentration relationship range from 0.1 to 10 $\mu\text{g L}^{-1}$.

1. Introduction

Aflatoxin is produced by *Aspergillus flavus* and *Aspergillus parasiticus*. Aflatoxin, mainly including B1, B2, G1, and G2, can cause acute

hepatitis, hemorrhagic necrosis, and growth disorders [1,2]. Among them aflatoxin B1 (AFB1) has attracted widespread attention and the International Agency for Research on Cancer (IARC) have placed it on the list as a class I carcinogen [3–5]. The contamination of AFB1 in foods

* Corresponding authors.

E-mail addresses: wangfeng@shnu.edu.cn (F. Wang), hfyang@shnu.edu.cn (H. Yang).

<https://doi.org/10.1016/j.saa.2022.122130>

Received 28 August 2022; Received in revised form 24 October 2022; Accepted 14 November 2022

Available online 28 November 2022

1386-1425/© 2022 Elsevier B.V. All rights reserved.

and feeds accounts for 75 % of the total mycotoxin contamination [6]. Many countries have established strict limitation for AFB1 in foodstuffs (AFB1 in cereals and their products, China: 5 µg/L, EU: 2 µg/L) [7,8]. Therefore, it calls for developing novel method with sensitivity and selectivity to monitor AFB1 levels.

Liquid chromatography–tandem mass spectrometry (LC–MS) [9] and high-performance liquid chromatography–tandem mass spectrometry (HPLC–MS) [10] to determinate AFB1 have been explored, which achieving high selectivity, sensitivity and precision. However, expensive equipment and skilled technician are needed for those methods. Alternatively, enzyme-linked immunosorbent assay (ELISA), colorimetric immunoassay, and fluorescence sensor are simple and rapid but they are susceptible to interference from the complex substrates in real samples [11–13].

Surface Enhanced Raman Spectroscopy (SERS) is a powerful detection method that can enhance the chemical “fingerprint” signals of target molecules by a million times when the molecules locating the vicinity of surface of noble metal nanostructures [14]. However, SERS method confronts many challenges including poor affinity of organic analyte to noble metal substrate and interference in complicated sample system [15]. In literature, there are many reports to improve the specificity of SERS detection by introduction of antibody, aptamer, and molecularly imprinted polymers (MIPs) [16,17]. For instance, Chen et al. used NH₂-DNA1-CS-Fe₃O₄ and SH-DNA2-ADANRs as enrichment nanoprobe and reporter nanoprobe respectively to develop SERS aptamer sensor for AFB1 and a limit of detection (LOD) at 0.0036 ng mL⁻¹ was reached [18]. However, pH and salt concentration had to be strictly controlled. Fang et al. fabricated magnetic Ni@Au core-shell nanoparticles to realize ultrasensitive competition magnetic immunoassay SERS assay for AFB1 and LOD was around 0.05 fg mL⁻¹ [19]. However, the detection reproducibility needs to be further improved.

Molecularly imprinted polymers (MIPs) are a kind of selective capture polymers with three-dimensional (3D) cavities after template removal. For selectively rebinding target molecule, chemical composition adaptation, spatial size adaptation, and spatial shape adaptation contribute to the high specific affinity of MIPs [20]. MIPs as artificial antibodies have received extensive concern due to low cost, reusable possibility, ease of use and large-scale separation/purification capability. The MIPs regarded as an efficient solid phase extraction (SPE) sorbents [21] have been widely applied in HPLC analysis [22]. The detection of AFB1 by using MIP technology combined with electrochemical methods [23,24], surface plasmon resonance (SPR) [25], and plasmon-enhanced fluorescence (PEF) [26] was also explored.

With the development of quantum chemistry and computers, molecular simulation methods were established to screen monomers to optimize MIPs synthesis [27,28]. Many software programs such as Hyper Chem [29], Gaussian 03 [30], and Discovery Studio [31] are commercially available to easily screen monomers based on ab initio [32,33], semiempirical [34,35] and density functional theory (DFT) [36,37]. However, such electron level calculations are time-consuming. Molecular simulation at a molecular level such as Discovery Studio takes short machine time, showing high degree of agreement between the calculations and the actual results [38] but previously reported MIPs based on DS simulations showed low recovery [39].

In this work, by using 7-ethoxycoumarin (7-EOC) as an analogue of aflatoxin, dummy molecular imprinting-solid phase extraction (DMIP-SPE) column was prepared. With the aid of molecularly design, both of optimal monomer and ratio of monomer and template were screened. The resultant AFB1-DMIP was employed as sorbents for separation and enrichment of AFB1. Thioctic acid assembled Ag NPs monolayer film (TA-Ag NPs MF) was prepared as SERS-active substrate. The DMI-SPE-based SERS sensor was adopted to analyze AFB1 in extract of peanut samples, exhibiting high selectivity, sensitivity and good detection reproducibility.

2. Experimental section

2.1. Materials and instruments

Methacrylic acid (MAA), 4-vinylpyridine (4-VP), *N*-isopropyl acrylamide (NIPAM), ethylene glycol dimethacrylate (EGDMA), 2,2'-azobisisobutyronitrile (AIBN), silver nitrate (AgNO₃, greater than 99 %), acrylic acid (AA), acrylamide (AM), 2-vinylpyridine (2-VP), 7-ethoxycoumarin (7-EOC), dodecanethiol (DDT), thioctic acid (TA), aristolochic acid I (AAI), patulin (PAT) and benzopyrene (B[a]P) were purchased from Sigma-Aldrich (USA). deoxynivalenol (DON), ochratoxin A (OTA), and aflatoxin G1 (AFG1) were purchased from Pribolab (China). Aflatoxin B1 was obtained from Yuanye Bio. Chloroform, acetonitrile, and methanol were bought from Shanghai Chemicals Ltd. Deionized water (18 MΩ cm) used in this work was acquired by a Millipore Direct-Q system. All glassware was cleaned with piranha solution (H₂SO₄:H₂O₂ = 7:3) and then thoroughly rinsed with deionized water.

Scanning electron microscope (SEM) images were obtained from Hitachi Su8220, operating at 10.0 kV. UV–vis spectra were collected by using a UV-6300PC double-beam spectrophotometer (VWR (Shanghai) Co., Ltd.). FTIR spectra of the DMIP and NIP were obtained using a FTIR spectrometer (Nicolet iS5, Thermo Fisher Scientific, USA). The porous structure of DMIP and NIP was characterized by a BET specific surface area analysis tester (JW-DA, Beijing JWGB SCI&Tech Co., Ltd). Raman spectra were acquired by using a Jobin Yvon confocal laser Raman system (Super LabRam II), which was equipped with a 10 × microscope lens and a He-Ne laser at 632.8 nm, and each spectrum was obtained by a scanning time of 8 s and 3 times accumulations. Agilent1100 high performance liquid chromatograph meter with chromatographic column DDS-C18 (4.6 × 250 mm, 5 µm) was employed for composition analysis.

2.2. Molecular design

All molecular simulations were conducted by Discovery Studio (DS, v3.0). The structures of commonly used functional monomers (AA, MAA, 2-VP, 4-VP, AM, NIPAM), dummy templates (7-EOC) as well as AFB1 were optimized by the Minimization module in DS. Their initial conformations and the potential energies (Table S1) were obtained by steepest descent and conjugate gradient methods for 2000 steps, respectively. 7-EOC or AFB1 was set as a receptor and a sphere with radius of 9.79 Å was set as the docking area. Then the half-flexible docking CDOCKER was applied to explore the interaction between receptor and ligand. In this process, high-temperature kinetic was applied to search the best conformation of the ligand, and the binding conformation was optimized through simulating annealing. The most stable template-monomer complex was selected and template-ligand interaction energy (ΔE) was calculated by following equation (1) [40]:

$$\Delta E = E_{\text{complex}} - E_{\text{template}} - nE_{\text{monomer}} \quad (1)$$

where E_{complex} is total energy of the complex and n refers to monomer number in the complex, E_{template} and E_{monomer} are the potential energies of the template and a functional monomer after minimization, respectively. Based on simulation results, the monomer with the strongest interaction with dummy template was preliminarily selected, and the optimal ratio of monomer to template was also tentatively determined.

2.3. Synthesis of DMIPs

MAA, 4-VP, and EDGMA were purified by vacuum distillation. NIPAM was purified through recrystallization prior to use. Bulk polymerization technique was applied to synthesize six different DMIPs using non-covalent approach. Briefly, 0.15 mmol 7-EOC and appropriate dosage of MAA ($n_{7\text{-EOC}}:n_{\text{MAA}} = 1:4$ or $1:5$), 4-VP ($n_{7\text{-EOC}}:n_{4\text{-VP}} = 1:4$ or $1:5$) and NIPAM ($n_{7\text{-EOC}}:n_{\text{NIPAM}} = 1:4$ or $1:5$) were dissolved in 1.5 mL

chloroform, respectively. The interaction of 7-EOC with monomer was performed at 25 °C for 2 h under stirring. Afterwards, 1.5 mmol cross-linker EDGMA and 5 mg initiator AIBN were added into the mixture under sonication. After purged with nitrogen for 10 min, the mixture was sealed and placed under ultraviolet irradiation (365 nm, 15 W) at a 4 cm distance from the light source to perform the polymerization. The formed bulk polymer was then taken out and crushed to a fine powder in a mortar. Finally, dummy template was removed via Soxhlet extraction with 150 mL methanol/acetic acid (9:1, v/v) for 16 h followed by washing with 150 mL methanol. After examining the UV band at 324 nm to ensure that the dummy template was completely removed, the polymer was dried in a vacuum chamber at 55 °C. As a control, the non-imprinted polymers (NIPs) were fabricated by the same procedure in the absence of dummy template.

2.4. Adsorption experiment

2.4.1. Adsorption capacity and selectivity

The adsorption capacity of the DMIPs and NIPs were examined by using 7-EOC in methanol solution (50 %, v/v). Specifically, 10 mg DMIPs or NIPs were mixed with 6 mL 7-EOC solution (10 mg/L) and then the mixture were shaken at 100 rpm for 2 h at ambient condition to ensure saturation. After centrifuged at 4000 g at 25 °C for 5 min, the unbound 7-EOC in the supernatant was measured at 324 nm by UV-vis spectrometer. The adsorption capacity at equilibrium (Q_e) was then characterized according to equation (2):

$$Q_e = \frac{(C_0 - C_e)V}{m} \quad (2)$$

where C_0 represents the initial concentration of 7-EOC (mg/L), C_e is the final concentration (mg/L) of 7-EOC remaining in solution after the adsorption process, V is the volume (mL) of solution and m refer to the dry weight of the DMIPs or NIPs (mg).

The selectivity of the prepared DMIPs was evaluated by the calculation of imprinting factor (IF, α) according to the equation (3):

$$\alpha = \frac{Q_{DMIPs}}{Q_{NIPs}} \quad (3)$$

where Q_{DMIPs} and Q_{NIPs} refer to the equilibrated adsorption capacity of DMIPs and NIPs for 7-EOC, respectively.

2.4.2. Static adsorption test

A series of 10 mg DMIPs or NIPs was added to 6 mL 7-EOC solution at different initial concentrations (C_0 : 2.5, 5, 7.5, 10, 12.5, 15, 25, 30, and 40 mg/L). After 2 h of shaking the equilibrium adsorption capacity was determined as described in Section 2.4.1. Scatchard isotherm model, Langmuir model and Freundlich model were further build by the following equations:

$$\frac{Q_e}{C_0} = -\frac{Q_{max}}{K_d} + \frac{Q_e}{K_d} \quad (4)$$

$$\lg Q_e = \lg K_F + \frac{\lg C_e}{n} \quad (5)$$

$$\frac{C_e}{Q_e} = \frac{C_e}{Q_{max}} + \frac{1}{K_L Q_{max}} \quad (6)$$

where K_d is the equilibrium dissociation constant of the binding site; Q_{max} is the maximum apparent binding amount of the binding site; n and K_F are the Freundlich adsorption intensity and indicators of adsorption capacity, respectively. K_L is Langmuir equilibrium constant.

2.4.3. Dynamic adsorption test

In the dynamic adsorption experiment, 10 mg of DMIPs or NIPs was added into 10 mL tubes, respectively, and mixed with 6 mL of 10 mg/L

7-EOC solution. The solutions were shaken at 100 rpm for 5, 10, 15, 20, 30, 45, 60, 90 and 120 min, respectively. Afterwards, pseudo-first-order kinetic equation and pseudo-second-order kinetic equation were employed to further study the kinetic data:

$$\ln(Q_e - Q_t) = \ln Q_e - K_1 t \quad (7)$$

$$\frac{t}{Q_t} = \frac{1}{K_2 Q_e^2} + \frac{t}{Q_e} \quad (8)$$

where Q_t and Q_e are adsorbed at time t and equilibrium respectively. K_1 and K_2 are the rate constants of pseudo-first-order and second-order adsorption processes, respectively.

2.5. Preparation of SERS substrate

2.5.1. Synthesis of Ag nanoparticles

Ag nanoparticles (AgNPs) were synthesized according Fren's method [41]. Briefly, 0.15 mM AgNO₃ was mixed with 150 mL ultrapure water in a 250 mL conical tube. Then the mixture was heated to boiling for 10 min under magnetic stirring and subsequently slowly added with 3 mL of 1 % trisodium citrate solution. After 30 min of continuous heating and stirring, the solution changes from colorless to grayish green. After cooling under ambient condition, AgNPs with average size of 50 nm in diameter were prepared.

2.5.2. Preparation of TA-AgNPs MF SERS substrates

4 mL acetone was firstly added into 4 mL Ag colloid suspension and shaken for a few seconds. Then, 4 mL of hexane containing certain amount of TA (10, 50, 100, 200, and 400 μ L) was rapidly added to the suspension. The mixture was transferred into a 50 mL beaker with 30 mL water. AgNPs assembled into a close-packed film at water/hexane interface in less than a minute. After complete evaporation of hexane, AgNPs film could be easily collected on quartz slide. This TA-AgNPs MF was used as an effective SERS substrate for analysis of AFB1 in peanuts eluent.

2.6. Sample pretreatment of peanuts

Fresh peanuts were purchased from local supermarket and crushed. 2.5 g sample was taken out to mix with 100 mL of 60:40 methanol/0.1 M KH₂PO₄ buffer (pH = 7.4). The mixture was then ultrasonicated for 10 min under ice bath condition. Afterwards, the extract solution was centrifuged at 4000 rpm for 5 min and the supernatant was filtered through a membrane. The extract was used for DMISPE procedure directly.

2.7. Ultrasound assisted DMISPE-SERS detection

The ultrasound assisted DMISPE for AFB1 was performed according to the Jayasinghe's report with some modifications [42]. Specifically, 100 mg DMIPs or NIPs were added into 10 mL of the above extract solution, and then shaken at 100 rpm for 20 min at room temperature. After centrifugation for 10 min at 8000r/min, DMIPs and NIPs were washed with 6 mL methanol to remove impurities and unimprinted AFB1. Subsequently, 3 mL 9:1 methanol/acetic acid mixture was ultrasonic treated for 15 min, and eluent was eluted for 3 times in total. The final eluent was dried under vacuum and then dissolved in 200 μ L methanol. 5 μ L of such solution was dropped on TA-AgNPs MF surface to conduct SERS detection after naturally drying.

3. Results and discussion

Fig. 1 illustrates the schematic DMISPE-SERS sensing system for determination of AFB1. First, molecular simulation is performed to select the most suitable monomer within acidic, neutral, and basic

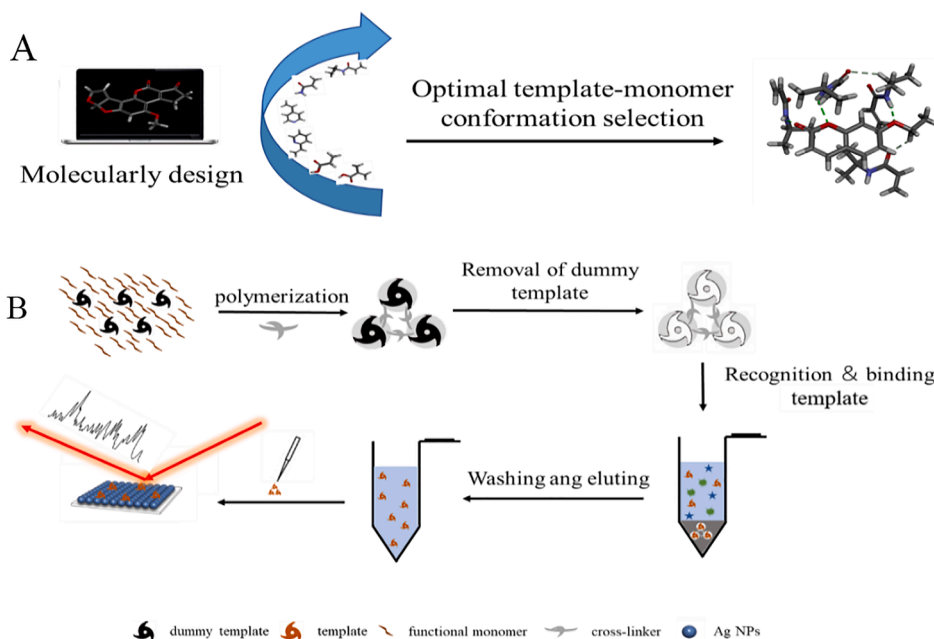


Fig. 1. Schematic illustration of molecular simulation (A) and DMISPE-SERS biosensor for the detection of AFB1 (B).

monomers including AA, MAA, AM, NIPAM, 2-VP, and 4-VP. Guided by the calculation results, NIPAM shows the strongest interaction with the template and is chosen as an optimal monomer to synthesize DMIPs for solid phase extraction. AFB1 is then isolated and enriched by DMISPE and is finally detected by the self-assembled TA-AgNPs MF SERS

substrate.

3.1. Molecular simulation

To overcome the problem of high-cost and toxicity of AFB1 as well as

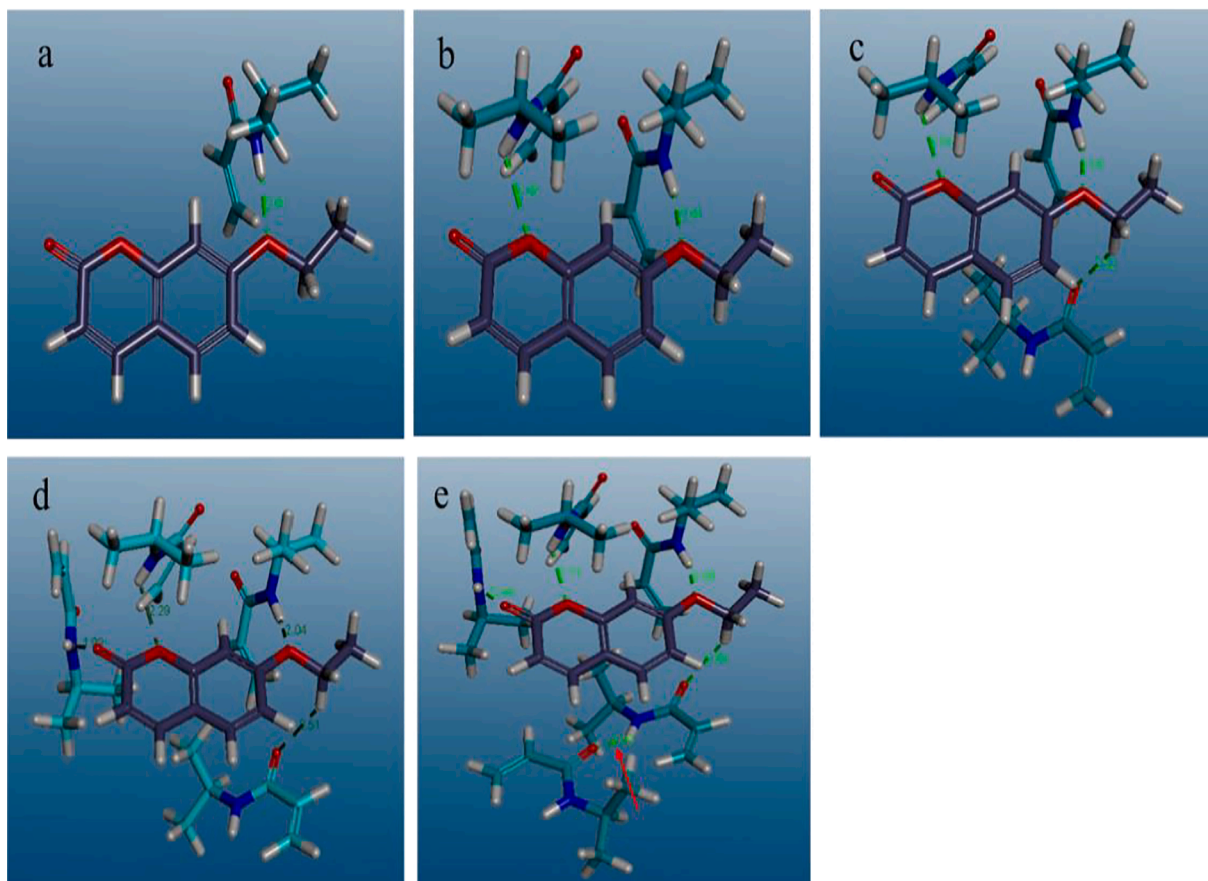


Fig. 2. The interaction patterns between NIPAM and 7-EOC in the ratio of 1:1 to 1:5.

to avoid template leakage, dummy template was put forward [43]. As AFB1 is a derivative of dihydrofuran coumarins, 7-EOC with a core structure like that of AFB1 is picked out as the dummy template to synthesize DMIPs (Fig. S1).

As the selective adsorption of DMIPs mainly depends on the interaction between functional monomer and template, appropriate type of functional monomer and the ratio of template to monomer are crucial for improving the performance of MIPs. Table S2 depicts the interaction energy values of 7-EOC-functional monomer complexes with different molar ratio. It can be found that the interaction energy gradually increases with the increase of monomer/template ratios and NIPAM, AM, and 4-VP shows greater interaction with 7-EOC compared to AA, MAA and 2-VP. It is also clear that at any template/monomer ratio, the interaction of NIPAM to template molecule shows the strongest one.

We further investigate the interaction pattern during template/monomer interaction. Taking NIPAM-7-EOC as an example system (Fig. 2 and Fig. S2), as the ratio of template to NIPAM increases from 1:1 to 1:4, the total number of hydrogen bonds and the total interaction energy increase. However, when the ratio of template to NIPAM reaches to 1:5, the 5th NIPAM interacts with NIPAMs which have already bound to template, implying that too high monomer-to-template ratio results in the redundant monomer units, which might increase the non-specific adsorption sites after polymerization. We therefore set the optimal 7-EOC/NIPAM ratio to be 1:4. In addition, as the ratio of template to 4-VP increases from 1:1 to 1:5, each 4-VP monomer tends to interact with template but the total interaction energy was weak.

Average interaction energy referring to the average energy contributed by each monomer at the optimal ratio of template and monomer, was introduced to reflect the specificity of MIPs. Fig. S3 is comparison for the average interaction energies for observed monomers. Clearly, the highest interaction energy ($12.85 \text{ kJ mol}^{-1}$) is achieved between 7-EOC and NIPAM. Consequently, we selected NIPAM as the functional monomer and a 1:4 template/monomer ratio to fabricate MIPs for construction of favorable recognition cavities with selective enrichment capacity.

To further confirm the feasibility of 7-EOC as dummy template for AFB1 imprinting, the interaction between the selected functional monomers and AFB1, the interaction between the selected functional monomers and 7-EOC, were studied respectively. CDocker module in DS software was used for the finding of optimal conformation of template/monomer interaction and the interaction energies are shown in Table 1. When the ratio of template to monomer was selected as 1:4, interaction energies of 7-EOC with functional monomers of MAA, AM and NIPAM were found to be -30.19 , -46.72 and -51.41 kcal/mol , respectively, while interaction energies of AFB1 with function monomers of MAA, AM and NIPAM are -33.56 , -48.77 and -52.09 kcal/mol , respectively, suggesting that all monomers have similar capability to bind AFB1 compared with 7-EOC as dummy template (Fig. S4).

3.2. Synthesis of DMIPs

To validate the simulation results, DMIPs were synthesized by using 7-EOC as the dummy template as well as NIPAM, MAA, and 4-VP as

Table 1

The interaction energies of the selected monomers with 7-EOC and with AFB1 in the ratio of 4:1.

Monomer	Interaction energy ($-\text{kcal/mol}$)	
	7-EOC	AFB1
AA	26.67	36.79
MAA	30.19	33.56
AM	46.72	48.77
NIPAM	51.41	52.09
2-VP	31.41	45.35
4-VP	37.56	46.21

monomers with different monomer/template ratios. To ensure uniformity during imprinting, 7-EOC was dissolved in chloroform, which acted as both a solvent and a porogen. The adsorption capacity of DMIPs and NIPs for 7-EOC together with the imprinting factor (IF) are tabulated in Table 2A. As expected, NIPAM-DMIPs exhibits higher adsorption capacity than (4-VP)-DMIPs and MAA-DMIPs due to the greater binding energy between NIPAM and 7-EOC. In case of 7-EOC to NIPAM ratio at 1:4, NIPAM exhibits the highest selectivity with IF of 2.32. For 4-VP, the adsorption capacity of (4-VP)-DMIPs is strong but the selectivity is unfavorable. In addition, NIPAM₅-DMIPs have better adsorption capacity than NIPAM₄-DMIPs but a smaller IF, which is consistent with the simulation results. As shown in Table 2B, similarly, when AFB1 to NIPAM ratio set at 1:4, NIPAM exhibits the highest selectivity with IF of 2.19. Consequently, the NIPAM₄-DMIPs are used to prepare the DMIPs-SPE column in next study.

3.3. Characterization of NIPAM₄-DMIPs

FTIR spectra of DMIPs, NIPs, cross-linker EGDMA and NIPAM were acquired. In Fig. S5, for NIPAM, FTIR bands at 1245 and 1533 cm^{-1} are assigned to the N—H bending of amide III and amide II bands. The FTIR peaks at 1624 and 1641 cm^{-1} are attributed to the stretching of the C=C and the asymmetric stretching of C=O in the amide I band, respectively. FTIR bands at 3290 and 3445 cm^{-1} are attributed to the N—H stretching. Notably, similar adsorption bands appear in the spectra of DMIPs and NIPs and the FTIR peak at 1624 cm^{-1} from C=C of NIPAM disappear after polymerization into DMIPs, while a novel peak at 1725 cm^{-1} due to stretching of C—O in EDGMA occurs. Clearly, EGDMA and NIPAM participate in the fabrication of DMIPs. Additionally FTIR signals of the NIPs are similar to those of the DMIPs [44,45].

For the preparation of DMIPs, the ratio of dummy template, monomer and cross-linker is 1:4:10, and the cross-linking usage has little effect on the pattern of monomer/template. Taking NIPAM₄-(7-EOC) system as an example (Fig. S6), computer simulation shows that EGDMA can effectively interact with the NIPAM₄-(7-EOC) pre-assembled structure via the hydrogen bonds and hardly break the structure. The cross-linker EGDMA distributed in the pre-assembled system presents the average interaction energy of $-4.81 \text{ kcal mol}^{-1}$, which is much smaller than the average interaction between NIPAM and 7-EOC ($-12.85 \text{ kcal mol}^{-1}$). Therefore, it is also worth stressing that crosslinker should be added after sufficient interaction between monomer and template molecules for 2 h.

SEM was used to characterize polymer morphology. In Fig. S7, compared to NIPs, DMIPs has uniform porous structures. Nitrogen

Table 2

Adsorption capacity of DMIPs and NIPs towards 7-EOC (A) and AFB1 (B) synthesized from three monomers to templates with different ratios.

A					
Monomer	Ratio of 7-EOC to functional monomer	Q _{DMIPs} ($\mu\text{g g}^{-1}$)	Q _{NIPs} ($\mu\text{g g}^{-1}$)	IF	
MAA	1:4	243	163	1.49	
	1:5	278	223	1.24	
NIPAM	1:4	430	185	2.32	
	1:5	483	265	1.82	
4-VP	1:4	345	188	1.83	
	1:5	436	228	1.91	
B					
Monomer	Ratio of AFB1 to functional monomer	Q _{DMIPs} ($\mu\text{g g}^{-1}$)	Q _{NIPs} ($\mu\text{g g}^{-1}$)	IF	
MAA	1:4	432	276	1.56	
	1:5	478	292	1.63	
NIPAM	1:4	678	309	2.19	
	1:5	692	368	1.88	
4-VP	1:4	486	285	1.35	
	1:5	518	292	1.43	

adsorption-desorption experiment was conducted to investigate the porosity of DMIPs and NIPs. Fig. S8 confirms that DMIPs has mesopores and greater porosity than NIPs [46,47], which could provide more imprinting sites and larger surface area for better specific adsorption of template molecules.

3.4. Adsorption properties of DMIPs and NIPs

Molecular recognition of MIPs can be illuminated by adsorption amount. Static adsorption isotherm of DMIPs (Fig. S9A) indicates it is mainly specific binding. DMIPs shows higher 7-EOC adsorption amount compared with NIPs. The kinetics adsorption curves are shown in Fig. S9B. With the increasing of adsorption time, the adsorption amount of MIPs increases rapidly and then achieves equilibrium within 20 min. DMIPs exhibit a greater adsorption capacity than NIPs, which corroborate specific recognition sites formed on the surface of DMIPs. In addition, the binding capacity of DMIPs toward 7-EOC was further determined by building Scatchard, Langmuir, and Freundlich modules (Fig. S10) [48]. The resulting parameters and equations for rebinding of 7-EOC onto the DMIPs are listed in Table S3. In Scatchard isotherm model (Fig. S10A), a straight line is obtained when 7-EOC binds on DMIPs, indicating one class of binding sites in DMIPs. The equilibrium dissociation constant K_d and the maximum saturated adsorption capacity Q_{max} are of $25.64 \mu\text{g mL}^{-1}$ and 1.6 mg g^{-1} , respectively.

The Langmuir isotherm model (Fig. S10B) is considered to have greater potential for describing the adsorption process, with the fitting correlation coefficient of 0.9924. The correlation parameters K_L of DMIPs also indicates an excellent imprinting effect due to the abundance binding sites on the MIPs. Meanwhile, the n value (adsorption intensity index) calculated from the Freundlich model (Fig. S10C) is 1.33 to DMIPs, suggesting that the 7-EOC could be easily captured by DMIPs.

Furthermore, the pseudo-first-order model and pseudo-second-order model were built to evaluate the adsorption mechanism of 7-EOC on DMIPs [49]. The kinetic models and corresponding parameters are provided in Fig. S11 and Table S4. The results suggest that the second-order kinetic equation with a high correlation coefficient of 0.98 could be better fit for the adsorption of 7-EOC on DMIP, indicating adsorption kinetics are mainly controlled by chemistry effect rather than by the material transport step.

The selective adsorption of the DMIPs and NIPs to AFB1 were also evaluated by choosing AAI, PAT and B[a]P as competitors. Under the same experimental conditions, in Fig. 3A, DMIPs show preferential adsorption to AFB1. The adsorption capacity of DMIPs to AFB1 is much more than that of its competitors. On the contrary, NIPs bearing no

specific recognition sites have poor adsorption selectivity. Moreover, IF of MIP to AFB1 is higher than the other competitive molecules.

The reusability of DMIPs was evaluated through repeating adsorption and desorption experiments. The desorption procedure was conducted in a Soxhlet apparatus to remove the adsorbed AFB1. In Fig. 3B, the recovery remains 90.3 % of the initial value at the 5th adsorption-desorption cycles, demonstrating excellent reusable owing to no adsorption capacities lost for AFB1. The simple, rapid, reliable, and reusable DMIPs have practically feasible for highly selective and sensitive analysis of AFB1 in complicated system.

3.5. Performance of DMISPE

Peanut extract still contains other components that interfere with detection of AFB1. Hence, the DMISPE procedure was performed to purify and enrich AFB1. To evaluate the extraction efficiency, the recovery of AFB1 from peanut extract and DMISPE/NISPE (non-imprinted solid-phase extraction) were confirmed by using HPLC method. In Table S5, a satisfied recovery of AFB1 by using DMISPE is more than 88 % while approximately half loss of the AFB1 if peanut extract is treated with NISPE. Besides, high AFB1 concentration in peanut extract results in decrease of recoveries even if DMISPE processes, attributed to the saturation adsorptions.

3.6. SERS determination of AFB1 in peanut

The self-assembly and transfer process for preparing TA-AgNPs MF is illustrated in Fig. S12. In detail, the stability of negatively charged citrate wrapped AgNPs is reduced by adding acetone [50]. A hexane solution containing TA is added under vigorous shaking to facilitate the replacement of citrate on the surface of AgNPs via thiolate interaction. The grayish green colloidal solution turns colorless after AgNPs accumulate to the hexane/water interface to form close-packed array (Fig. S13). TA on the surface of AgNPs provides hydrogen bond interaction to enrich AFB1. As a result, DMISPE-SERS sensor exhibits sensitive and selective determination of AFB1.

We investigated the interactions of AFB1 with TA and DDT by simulation, respectively and for the convenience of theoretical calculation, S atom was replaced with C atom. In Fig. S14, two hydrogen bonding interactions ($-12.75 \text{ kcal mol}^{-1}$) between carboxyl group of TA and carbonyl groups of AFB1 is greater than hydrophobic interaction ($-8.86 \text{ kcal mol}^{-1}$) between DDT and AFB1. Modification of TA on the AuNPs array effectively trapped the AFB1 molecule to allow enhancement of Raman scattering.

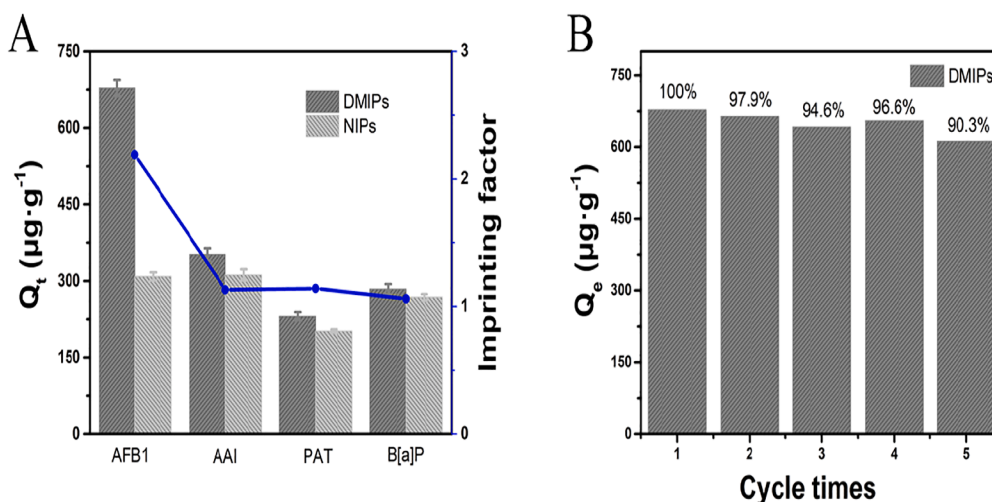


Fig. 3. The selectivity of DMIPs and NIPs towards AFB1 and its competitors (AFB1, AAI, PAT and B[a]P of 10 mg/L respectively in methanol/ H_2O solution) (A). Recycling experiments of MIP over five cycles of adsorption-desorption in methanol/ H_2O solution of AFB1 solution (B).

To obtain the optimal SERS signal, TA modification amount was observed by probe molecule R6G. In Fig. S15A and B, when TA usage is 100 μL , the best SERS signal of R6G is achieved. In Fig. S15C, SEM image recorded on AuNPs array modified with TA by using 100 μL shows an even and closely packed state. If further increasing TA volume to 500 μL , the disorder assembly could be visible in Fig. S15D.

As shown in Fig. S16A, low background Raman signal of TA-AgNPs MF [51] could be negligible in detection application. In Fig. S16B, characteristic peaks of R6G as low as 10^{-9} mol/L can still be clearly observed ($S/N > 3$), indicating TA-AgNPs MF-based SERS method has high detection sensitivity. The repeatability and stability of TA-AgNPs MF -SERS method was also carefully examined. In Fig. S17A and B, SERS spectra of R6G collected from 15 different points on one substrate proves good signal uniformity. Relative standard derivation (RSD) of SERS signals acquired on 6 different preparation batches of TA-AgNPs MF is 8.21 %, showing acceptable reproducibility (Fig. S17C and D). The storage stabilities of TA-AgNPs MF in different environments were also investigated. In Fig. S18, after storage in air for 1 month, the SERS intensity keeps 75.6 %. On the contrary, SERS intensity could remain 93 % in ethanol for 63 days.

SERS determination of AFB1 were performed on TA and DDT modified AgNPs MF. As shown in Fig. S19, DDT-AgNPs MF show high background interference and are not suitable for AFB1 detection. As a comparison, after TA-AgNPs MF substrate is incubated with 1 mg/L of AFB1 solution, stronger AFB1 signal could be reached while only weak SERS signal of AFB1 presents on DDT-AgNPs MF.

In Fig. S20, DMISPE-SERS showed the better SERS performance because DMIPs solid-phase could effectively extract AFB1 from pretreated solution. Characteristic peaks of AFB1 at 630, 684, 830, 1246, 1270, 1302, 1442, 1486, 1552, and 1592 cm^{-1} could be clearly visible and the assignment to Raman shifts [52,53] is summarized in Tables S6.

DMISPE-SERS spectra for AFB1 spiked in peanut with different concentrations were recorded and smoothing and automatic baseline correction were preprocessed. The concentration-dependent average SERS spectra are displayed in Fig. 4A. The distinctive SERS peak at 684 cm^{-1} due to C–H in-plane bending was chosen to plot the dynamic relationship between SERS intensities and AFB1 concentrations. A good linear relationship is found ($R^2 = 0.968$) ranging from 0.1 to 10 $\mu\text{g/L}$. Limit of detection (LOD) for AFB1 is 0.1 $\mu\text{g/L}$ by using DMISPE-SERS assay (Fig. 4B), which meets the requirements of European Union standards (2 $\mu\text{g/L}$). Clearly, DMISPE-SERS protocol should be an effective means to determine trace AFB1 in peanut.

The comparison with other methods previously reported in literature is tabulated in Table S7, including LOD and linear range. Obviously,

HPLC and QCM methods are better than DMISPE-SERS but they are not suitable for the on-site detection. Fluorescence methods suffers from background fluorescence and quenching effects. SERS technology combined with aptamer or antibody could detect low level of targeted analytes. However, strict pH and salt/buffer concentration are required, which might trigger the aggregation of SERS substrate and deteriorate the final SERS signal, the quality of antibodies between different batches is also a concern. Therefore, DISPE-SERS approach exhibits a promising merit in detection of AFB1 in real sample.

3.7. Detection of AFB1 in moldy samples

As peanuts are susceptible to contamination by mycotoxins such as DON, OTA and AFG1 with the similar structures (Table S8) to AFB1, which might interfere with the detection of AFB1. The Raman spectra of DON, OTA, AFG1 and AFB1 are shown in Fig. S21. DON and OTA have SERS peaks in the range of 2800–3200 cm^{-1} , while AFG1 has strong characteristic peaks at 570, 600, 658 and 710 cm^{-1} . AFB1 has strong Raman peak at 678 cm^{-1} , which is free from interferences of DON, OTA, AFG1.

Moldy peanuts were pretreated as described in experimental Section 2.6 followed by the selective adsorption of AFB1 by using DMISPE. The DMISPE extract was directly detected on TA-Ag NPs MF. In Fig. S22, SERS bands AFB1 at 684, 1552, and 1592 cm^{-1} are clearly visible. What's more, AFB1 was spiked fresh peanuts and detected by DMISPE-SERS assay in blind way. The moldy peanut extract was injected in HPLC with acetonitrile-methanol-water (1:1:2) as mobile phase, flow rate 1.0 mL/min, excitation wavelength at 360 nm; emission wave length of 450 nm, column temperature 30 $^{\circ}\text{C}$ to detect the AFB1. In Table S9, the SERS detection recoveries are ranging from 93 % to 102 % which are similar results from 97.8 % to 102 % obtained by HPLC method. DMISPE-SERS sensor has the advantages of easy sample pretreatment and on-site determination.

4. Conclusions

DMISPE-SERS sensor was developed for rapid, selective, and sensitive determination of AFB1 in peanut. Molecular simulation was performed to screen the best monomer, monomer/template ratio, and cross-linking agent for preparation optimal DMISPE, which having good adsorption selectivity toward AFB1. After DMISPE treatment, the adsorption recovery of AFB1 was greater than 88 %. In addition, after 5 adsorption-desorption cycles, the adsorption capacity of DMISPE could keep 90.3 % of the initial value. TA-AgNPs MF was prepared as SERS

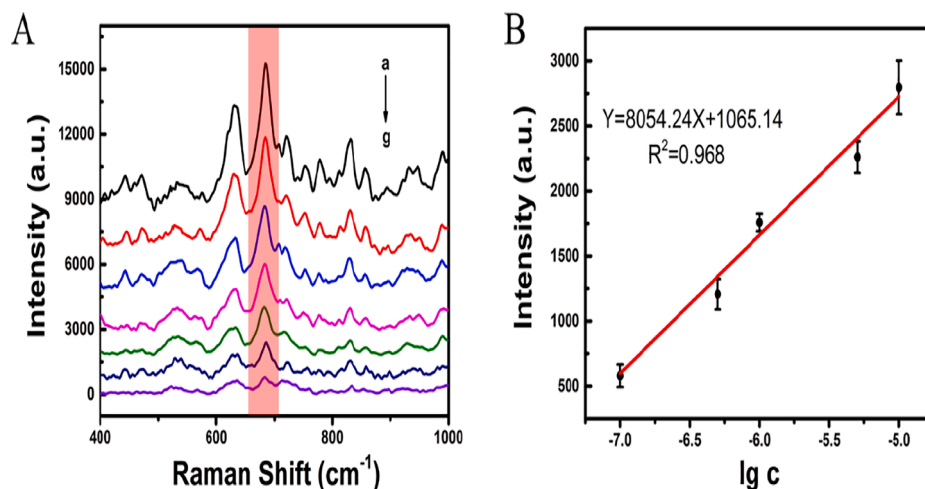


Fig. 4. (A) Representative DMISPE-SERS spectra of peanut samples spiked with different concentrations of AFB1 (a–g: 10^{-3} – 10^{-7} g/L); (B) the linear relationships between SERS intensity at 684 cm^{-1} from 0.1 to 10 $\mu\text{g/L}$.

substrate and SERS detectable concentration of R6G was as low as 10^{-9} mol/L with RSD of 5.96 %. After 63 days of storage in ethanol, the SERS signal remained 93 %, showing the reasonable stability. DMISPE-SERS assay was utilized to detect AFB1. A concentration linear relationship in the range of 0.1–10 $\mu\text{g L}^{-1}$ with LOD of 0.1 $\mu\text{g L}^{-1}$ could be achieved. The recoveries of SERS detection of AFB1 in peanut samples ranging from 93 % to 102 % exhibited great potential in the screening/quantification of biotoxins.

Declaration of Competing Interest

The authors declare that they have no known competing financial interests or personal relationships that could have appeared to influence the work reported in this paper.

Acknowledgments

This work is supported by the National Natural Science Foundation of China (no. 21475088), International Joint Laboratory on Resource Chemistry (IJLRC), Shanghai Key Laboratory of Rare Earth Functional Materials, and Shanghai Municipal Education Committee Key Laboratory of Molecular Imaging Probes and Sensors.

Appendix A. Supplementary material

Supplementary data to this article can be found online at <https://doi.org/10.1016/j.saa.2022.122130>.

References

- M. Díaz-Bao, P. Regal, R. Barreiro, C.A. Fente, A. Cepeda, A facile method for the fabrication of magnetic molecularly imprinted stir-bars: a practical example with aflatoxins in baby foods, *J. Chromatogr. A* 1471 (2016) 51–59, <https://doi.org/10.1016/j.chroma.2016.10.022>.
- K. Campbell, A.L. Ferreira Cavalcante, P. Galvin-King, M. Oplowska-Stachowiak, C. Brabet, I. Metayer, D. Montet, S.A. Haughey, C.T. Elliott, Evaluation of an alternative spectroscopic approach for aflatoxin analysis: comparative analysis of food and feed samples with UPLC–MS/MS, *Sens. Actuators B Chem.* 239 (2017) 1087–1097, <https://doi.org/10.1016/j.snb.2016.08.115>.
- L. Chen, F. Wen, M. Li, X. Guo, S. Li, N. Zheng, J. Wang, A simple aptamer-based fluorescent assay for the detection of Aflatoxin B1 in infant rice cereal, *Food Chem.* 215 (2017) 377–382, <https://doi.org/10.1016/j.foodchem.2016.07.148>.
- G. Xu, S. Zhang, Q. Zhang, L. Gong, H. Dai, Y. Lin, Magnetic functionalized electrospun nanofibers for magnetically controlled ultrasensitive label-free electrochemiluminescent immune detection of aflatoxin B1, *Sens. Actuators B Chem.* 222 (2016) 707–713, <https://doi.org/10.1016/j.snb.2015.08.129>.
- F. Waliyar, S.V. Reddy, P. Lava-Kumar, Review of immunological methods for the quantification of aflatoxins in peanut and other foods, *Peanut Sci.* 36 (1) (2009) 54–59, <https://doi.org/10.3146/AT07-007.1>.
- A.P. Wacoob, W. Deborah, P.C. Vuzi, J.F. Hawumba, Methods for detection of aflatoxins in agricultural food crops, *J. Appl. Chem.* (2014) 1–15, <https://doi.org/10.1155/2014/706291>.
- X. Ding, P. Li, Y. Bai, H. Zhou, Aflatoxin B1 in post-harvest peanuts and dietary risk in China, *Food Control* 23 (1) (2012) 143–148, <https://doi.org/10.1016/j.foodcont.2011.06.026>.
- B. Lin, P. Kannan, B. Qiu, Z. Lin, L. Guo, On-spot surface enhanced Raman scattering detection of Aflatoxin B1 in peanut extracts using gold nanobipyramids evenly trapped into the AAO nanoholes, *Food Chem.* 307 (2020), 125528, <https://doi.org/10.1016/j.foodchem.2019.125528>.
- A. Bacaloni, C. Cavaliere, F. Cucci, P. Foglia, R. Samperi, Determination of aflatoxins in hazelnuts by various sample preparation methods and liquid chromatography-tandem mass spectrometry, *J. Chromatogr. A* 1179 (2) (2008) 182–189, <https://doi.org/10.1016/j.chroma.2007.11.081>.
- W.S. Khayoon, B. Saad, T.P. Lee, B.J.F.C. Salleh, High performance liquid chromatographic determination of aflatoxins in chilli, peanut and rice using silica based monolithic column, *Food Chem.* 133 (2) (2012) 489–496, <https://doi.org/10.1016/j.foodchem.2012.01.010>.
- J. Chen, Q.-H. He, Y. Xu, J.-H. Fu, Y.-P. Li, Z. Tu, D. Wang, M. Shu, Y.-L. Qiu, H.-W. Yang, Y.-Y. Liu, Nanobody mediated immunoassay for ultrasensitive detection of cancer biomarker alpha-fetoprotein, *Talanta* 147 (2016) 523–530, <https://doi.org/10.1016/j.talanta.2015.10.027>.
- X. Guo, F. Wen, N. Zheng, Q. Luo, H. Wang, H. Wang, S. Li, J.J.B. Wang, Bioelectronics, development of an ultrasensitive aptasensor for the detection of aflatoxin B1, *Biosens. Bioelectron.* 56 (2014) 340–344, <https://doi.org/10.1016/j.bios.2014.01.045>.
- T. Li, J.Y. Byun, B. Kim, Y.B. Shin, M.G.J.B. Kim, Bioelectronics, Label-free homogeneous FRET immunoassay for the detection of mycotoxins that utilizes quenching of the intrinsic fluorescence of antibodies, *Biosens. Bioelectron.* 42 (2013) 403–408, <https://doi.org/10.1016/j.bios.2012.10.085>.
- L. Qi, M. Xiao, X. Wang, C. Wang, L. Wang, S. Song, X. Qu, L. Li, J. Shi, H.J. Pei, DNA-encoded Raman-active anisotropic nanoparticles for microRNA detection, *Anal. Chem.* 89 (18) (2017) 9850–9856, <https://doi.org/10.1021/acs.analchem.7b01861>.
- L. Jiang, M.M. Hassan, S. Ali, H. Li, R. Sheng, Q.J. Chen, Technology, evolving trends in SERS-based techniques for food quality and safety: a review, *Trends Food Sci. Technol.* 112 (2021) 225–240, <https://doi.org/10.1016/j.tifs.2021.04.006>.
- F. Wang, S. Cao, R. Yan, Z. Wang, D. Wang, H.J.S. Yang, Selectivity/specificity improvement strategies in surface-enhanced Raman spectroscopy analysis, *Sensors* 17 (12) (2017) 2689, <https://doi.org/10.3390/s17112689>.
- A.R. Bizzarri, S.J.A.S. Cannistraro, Surface-enhanced resonance Raman spectroscopy signals from single myoglobin molecules, *Appl. Spectrosc.* 56 (12) (2002) 1531–1537, <https://doi.org/10.1366/000370202321115977>.
- Q. Chen, M. Yang, X. Yang, H. Li, Z. Guo, M.H. Rahma, A large Raman scattering cross-section molecular embedded SERS aptasensor for ultrasensitive Aflatoxin B1 detection using CS-Fe₃O₄ for signal enrichment, *Spectrochim. Acta A Mol. Biomol. Spectrosc.* 189 (2017) 147–153, <https://doi.org/10.1016/j.saa.2017.08.029>.
- C. Fang, C. Wei, M. Xu, Y. Yuan, R. Gu, J. Yao, Ni@Au nanoparticles for surface enhanced Raman spectroscopy based ultrasensitive magnetic immunoassay on aflatoxin B1, *RSC Adv.* 6 (2016) 61325–61333, <https://doi.org/10.1039/c6ra09397c>.
- O.S. Ahmad, T.S. Bedwell, C. Esen, A. Garcia-Cruz, S.A. Piletsky, Molecularly imprinted polymers in electrochemical and optical sensors, *Trends Biotechnol.* 37 (3) (2019) 294–309.
- H.J.A. Karsten, Chemistry, peer reviewed: molecularly imprinted polymers: the next generation, *Anal. Chem.* 75 (17) (2003) 376A–383A, <https://doi.org/10.1021/ac031385h>.
- F. Puoci, G. Cirillo, M. Curcio, F. Iemma, U.G. Spizzirri, N.J.A.C.A. Picci, Molecularly imprinted solid phase extraction for the selective HPLC determination of α -tocopherol in bay leaves, *Anal. Chim. Acta* 593 (2) (2007) 164–170, <https://doi.org/10.1016/j.aca.2007.04.053>.
- S. Mugo, M. Wood, A MIP-enabled stainless-steel hypodermic needle sensor for electrochemical detection of aflatoxin B1, *Anal. Methods* 21 (14) (2022) 2063–2071, <https://doi.org/10.1039/D1AY02084F>.
- M. Roushani, S. Farokhi, Z. Rahmati, Development of a dual-recognition strategy for the aflatoxin B1 detection based on a hybrid of aptamer-MIP using a Cu₂O NCs/GCE, *Microchem. J.* 178 (2022), 107328, <https://doi.org/10.1016/j.microc.2022.107328>.
- S. Akgönüllü, H. Yavuz, A. Denizli, SPR nanosensor based on molecularly imprinted polymer film with gold nanoparticles for sensitive detection of aflatoxin B1, *Talanta* 219 (2020) 121219.
- T. Sergeeva, D. Yarynka, V. Lytvyn, P. Demydov, A. Lopatynskyi, Y. Stepanenko, O. Brovko, A. Pinchuk, V. Chegel, Highly-selective and sensitive plasmon-enhanced fluorescence sensor of aflatoxins, *Analyst* 147 (6) (2022) 1135–1143, <https://doi.org/10.1039/d1an02173g>.
- B.o. Gao, X.-P. He, Y. Jiang, J.-T. Wei, H. Suo, C. Zhao, Computational simulation and preparation of fluorescent magnetic molecularly imprinted silica nanospheres for ciprofloxacin or norfloxacin sensing, *J. Sep. Sci.* 37 (24) (2014) 3753–3759.
- A. Azimi, M.J.A.C.A. Javanbakht, Computational prediction and experimental selectivity coefficients for hydroxyzine and cetirizine molecularly imprinted polymer based potentiometric sensors, *Anal. Chim. Acta* 812 (2014) 184–190, <https://doi.org/10.1016/j.aca.2013.12.042>.
- L. Wu, Y.J.J. Li, Study on the recognition of templates and their analogues on molecularly imprinted polymer using computational and conformational analysis approaches, *J. Mol. Recognit.* 17 (6) (2010) 567–574, <https://doi.org/10.1002/jmr.688>.
- P. Li, F. Rong, Y. Xie, V. Hu, C. Yuan, Study on the binding characteristic of S-naproxen imprinted polymer and the interactions between templates and monomers, *J. Anal. Chem.* 59 (10) (2004) 939–944, <https://doi.org/10.1023/b:janc.0000043909.32186>.
- K. Zhang, W. Zou, H. Zhao, P. Dramou, C. Pham-Huy, J. He, H.J.R.A. He, Adsorption behavior of a computer-aid designed magnetic molecularly imprinted polymer via response surface methodology, *RSC Adv.* 5 (75) (2015) 61161–61169, <https://doi.org/10.1039/c5ra10367c>.
- E.M. Saad, N.A. El Gohary, M. Abdel-Halim, H. Handoussa, R. Mohamed El Nashar, B. Mizaikoff, Molecularly imprinted polymers for selective extraction of rosmarinic acid from *Rosmarinus officinalis* L., *Food Chem.* 335 (2021) 127644.
- Q. Gao, Y. Zang, Y. Zhang, J.u. Xie, J. Li, J. Gao, H. Xue, Composite polymerized molecular imprinting membrane-based electrochemical sensor for sensitive determination of curcumin by using 4-pentenoyl-aminoacyl-chitosan oligosaccharide as functional monomer oligomer, *J. Electroanal. Chem.* 879 (2020) 114793.
- F. Feng, J. Zheng, P. Qin, T. Han, D.J.T. Zhao, A novel quartz crystal microbalance sensor array based on molecular imprinted polymers for simultaneous detection of clenbuterol and its metabolites, *Talanta* 167 (2017) 94–102, <https://doi.org/10.1016/j.talanta.2017.02.001>.
- A. Wy, A. Yt, A. Ys, A. Wl, C. Swa, B.J.F.C. Xwa, Preparation of a carboxylated single-walled carbon-nanotube-chitosan functional layer and its application to a molecularly imprinted electrochemical sensor to quantify semicarbazide, *Food Chem.* 333 (2020), 127524, <https://doi.org/10.1016/j.foodchem.2020.127524>.
- Q. Zhou, M. Wang, S. Yagi, T.J.N. Minami, Extended gate-type organic transistor functionalized by molecularly imprinted polymer for taurine detection, *Nanoscale* 13 (2021) 100–107, <https://doi.org/10.1039/D0NR06920E>.

- [37] X. Yu, H. Zeng, J. Wan, X. Cao, Computational design of a molecularly imprinted polymer compatible with an aqueous environment for solid phase extraction of chenodeoxycholic acid, *J. Chromatogr. A* 1609 (2020) 460490.
- [38] W. Tang, L. Yin, J.R. Sempionatto, J. Moon, H. Teymourian, J.J.A.M. Wang, Touch-based stressless cortisol sensing, *Adv. Mater.* 33 (18) (2021) 2008465, <https://doi.org/10.1002/adma.202008465>.
- [39] G. Li, Z. Kai, M. Fizir, M. Niu, S. Cheng, S. Xi, X. Hui, J. Shi, H.J.N. Hua, Rational design, preparation and adsorption study of a magnetic molecularly imprinted polymer using a dummy template and a bifunctional monomer, *New J. Chem.* 41 (2017) 7092–7101, <https://doi.org/10.1039/c7nj00689f>.
- [40] M. Niu, C. Sun, K. Zhang, G. Li, F. Meriem, C. Pham-Huy, X. Hui, J.R. Shi, H.J. N. He, A simple extraction method for norfloxacin from pharmaceutical wastewater with a magnetic core-shell molecularly imprinted polymer with the aid of computer simulation, *New J. Chem.* 41 (7) (2017) 2614–2624, <https://doi.org/10.1039/c6nj03901d>.
- [41] G. Frens, Controlled nucleation for the regulation of the particle size in monodisperse gold suspensions, *Nat. Phys.* 241 (105) (1973) 20–22, <https://doi.org/10.1038/PHYS241020A0>.
- [42] G.D.T.M. Jayasinghe, R. Domínguez-González, P. Bermejo-Barrera, A. Moreda-Piñeiro, Ultrasound assisted combined molecularly imprinted polymer for the selective micro-solid phase extraction and determination of aflatoxins in fish feed using liquid chromatography-tandem mass spectrometry, *J. Chromatogr. A* 1609 (2020) 460431.
- [43] Y. Liang, J. He, Z. Huang, H. Li, Y. Zhang, H. Wang, C. Rui, Y. Li, L. You, K. Li, S. Zhang, An amino-functionalized zirconium-based metal-organic framework of type UiO-66-NH₂ covered with a molecularly imprinted polymer as a sorbent for the extraction of aflatoxins AFB1, AFB2, AFG1 and AFG2 from grain, *Microchim. Acta* 187 (1) (2020).
- [44] L. Surucic, A. Nastasovic, A. Onjia, G. Janjic, A. Rakic, Design of amino-functionalized chelated macroporous copolymer [poly(GMA-EDGMA)] for the sorption of Cu (II) ions, *J. Serbian Chem. Soc.* 84 (12) (2019) 1391–1404.
- [45] H.L. Wang, L. Pang, W.F. Jiang, C.J.C.C.L. Yang, Preparation and characterization of thermosensitive poly(NIPAM-co-MAH- β -CD)/(TiO₂-MWCNTs) composites by UV light photoinitiating method, *Chin. Chem. Lett.* 23 (9) (2012) 1071–1074, <https://doi.org/10.1016/j.ccllet.2012.05.028>.
- [46] Z. Wang, R. Yan, S. Liao, Y. Miao, B. Zhang, F. Wang, H.J.A.S.S. Yang, In situ reduced silver nanoparticles embedded molecularly imprinted reusable sensor for selective and sensitive SERS detection of Bisphenol A, *Appl. Surf. Sci.* 457 (1) (2018) 323–331, <https://doi.org/10.1016/j.apsusc.2018.06.283>.
- [47] B.M. Jung, M.S. Kim, W.J. Kim, J.Y. Chang, Molecularly imprinted mesoporous silica particles showing a rapid kinetic binding, *Chem. Commun. (Camb)* 46 (21) (2010) 3699–3701, <https://doi.org/10.1039/c003173a>.
- [48] Y. Xiao, R. Xiao, J. Tang, Q. Zhu, X. Li, Y. Xiong, X.J.T. Wu, Preparation and adsorption properties of molecularly imprinted polymer via RAFT precipitation polymerization for selective removal of aristolochic acid I, *Talanta* 162 (2017) 415–422, <https://doi.org/10.1016/j.talanta.2016.10.014>.
- [49] Y. Cui, W. Kang, L. Qin, J. Ma, X. Liu, Y. Yang, Magnetic surface molecularly imprinted polymer for selective adsorption of quinoline from coking wastewater, *Chem. Eng. J.* 397 (2020) 125480.
- [50] H. Tian, H. Li, Y.J.A.A.M. Fang, Interfaces, binary thiol-capped gold nanoparticle monolayer films for quantitative SERS analysis, *ACS Appl. Mater. Interfaces* 11 (2019) 16207–16213, <https://doi.org/10.1021/acsami.9b02069>.
- [51] Y. Lai, C. Wang, H. Shao, Thioctic acid-modified silver nanoplates on copper foil for low interference detection of fluoranthene by surface-enhanced Raman spectroscopy, *ACS Appl. Nano Mater.* 3 (2) (2020) 1800–1807, <https://doi.org/10.1021/acsanm.9b02496>.
- [52] X. Wu, S. Gao, J.S. Wang, H. Wang, Y.W. Huang, Y.J.A. Zhao, The surface-enhanced Raman spectra of aflatoxins: spectral analysis, density functional theory calculation, detection and differentiation, *Analyst* 137 (18) (2012) 4226–4234, <https://doi.org/10.1039/c2an35378d>.
- [53] J. Li, H. Yan, X. Tan, Z. Lu, H.J.A.C. Han, Cauliflower-inspired 3D SERS substrate for multiple mycotoxins detection, *Anal. Chem.* 91 (6) (2019) 3885–3892, <https://doi.org/10.1021/acs.analchem.8b04622>.